

Analytical modelling of a large-scale dynamic testing facility

P. Ceresa^{1, §}, F. Brezzi², G.M. Calvi³, R. Pinho³

¹European Centre for Training and Research in Earthquake Engineering (EUCENTRE), Pavia, Italy

²Istituto Universitario di Studi Superiori (I.U.S.S.), Pavia, Italy

³University of Pavia, Department of Structural Mechanics, Pavia, Italy

SUMMARY

An analytical model which aims at reproducing the response of a large-scale dynamic testing facility, that is a system composed by the specimen/shaking-table/reaction-mass/airbags/dampers/soil, is developed. The Lagrangian of the system is derived, under the assumption of large displacements and rotations. A set of four nonlinear differential equations is obtained and solved with numerical methods. Preliminary verifications of the derived model are carried out by reproducing both well-known results in literature as well as those of a lumped model employed in the design of an existing dynamic testing facility. The case-study for validating the nonlinear equations of motion is the shaking table of the EUCENTRE Laboratory.

Keywords: Lagrange's formulation; nonlinear kinematics; nonlinear differential equations of motion; Runge-Kutta methods; shaking table tests

1. INTRODUCTION

In order to reproduce historical earthquake ground motion using a seismic simulator, the dynamics of the simulator and test structure must be accounted for. Methods for the dynamic modelling of hydraulically actuated systems have been developed over a number of decades (e.g., see ref. [1]). Of those that have discussed the dynamics of seismic simulators, the number that has concentrated on the dynamics of uniaxial seismic simulators is relatively small (e.g., see ref. [2-14]). The likelihood that structural compliance in the test rig will affect performance has not often been considered. Moreover, reaction mass dynamics have been modelled in one case only [7], leading to a linear analytical model of a uniaxial, servo-hydraulic, stroke controlled shaking table system using jointly structural dynamics and linear control theory.

In the aforementioned references, there is a wide variation in the complexity of models and in the sophistication of the actuator feedback control system. The proposed research does not deal with the control of shaking tables, even if it is recognised that seismic testing of large structures presents a significant control challenge, and is the subject of academic research [10-14] as well as the application of advanced industrial control techniques [9]. This research aims at deriving a model capable of simulating the behaviour of a shaking table that could be subjected to possible large rotations. Therefore, this research study aims at formulating and studying a deterministic model which describes the behaviour of a large-scale dynamic testing facility including the effects of the interaction between the specimen/shaking-table/reaction-mass/isolation-damping-systems/foundation-soil. If the shaking table is a movable system in a rotating frame of reference, additional effects, such as the Coriolis' acceleration, could have a great influence on the expected response of the dynamic testing facility. Moreover, the complexity of the interaction between the shaking table and the movable support system depends on the dynamic impedances of the soil, on the stiffness coefficients related to the isolators, or even the damping coefficients of the dampers. The first objective of this study is the development of a model for a shaking table designed for performing single-axis tests but that could be affected by the motion (i.e., the rocking) of the reaction mass, resulting in a set of high-order nonlinear equations suitable for numerical solutions and applicable to a wide range of dynamic testing facilities. The proposed model is called nonlinear

 § Correspondence to: P. Ceresa, European Centre for Training and Research in Earthquake Engineering (EUCENTRE), Via Ferrata 1, 27100 Pavia, Italy. Phone: +39 0382 516962; Fax: +39 0382 529131; Email: paola.ceresa@eucentre.it

since it deals with nonlinear kinematics due to the possible rocking of the support system (i.e., reaction-mass/isolation-damping-systems/foundation-soil). The nonlinear kinematics is considered in the formulation since a large rotation associated with an intended uniaxial input could have a very strong influence on the response of the shaking table and the specimen. A further objective is the validation of the model identifying the parameters that mainly affect the facility response. Finally, this research aims at being useful for understanding the causes of the complex behaviour of a large dynamic testing facility and helping in future experimental campaigns. In order to reach these objectives the present work is organised in the different phases, described in the following sections: (i) derivation of the Lagrangian of the dynamic system, assuming large displacements, (ii) preliminary verifications of the developed model deriving well-known results in literature and studying the accuracy of both equations and numerical solver, (iii) preliminary validations of the analytical solutions with the measured responses of the large-scale shaking table of the EUCENTRE Laboratory [15].

2. ANALYTICAL MODEL DERIVATION

The development of a dynamic model (i.e. the mathematical description) of the system to be controlled is fundamental for reaching the overall goal of feedback control. As stated by Franklin et al. [16], the term model, as it is used and understood by control engineers, means a set of differential equations that describe the dynamic behaviour of the system. The use of Lagrange's equation provides a systematic unified approach for handling a broad class of physical systems, no matter how complex in structure they may be [17]. For this reason, the latter is applied for deriving the equations of motion of a large-scale dynamic testing facility, as presented in the next sections.

The dynamic testing facility herein considered refers to a typical large shaking table system that is a platform excited with servo-hydraulic actuators (Fig. 1a) to generate artificial earthquakes and other dynamic testing signals of interest in the laboratory. The platform structure is most commonly a welded up steel structure with torsionally stiff shell and internal stiffening honeycomb (Fig. 1b). The specimen to be tested is fixed to the table surface with preloaded bolts and tie rods. The servo-hydraulic actuator is designed for low friction with full angular swivelling spherical bearings at the head and base. The reaction mass is constructed of reinforced concrete. Some site conditions allow the reaction mass to rest directly on the supporting soil, but for environmental and neighbourhood considerations, the reaction mass is often isolated by air suspension springs and damped by heavy duty automotive shock absorbers [18].

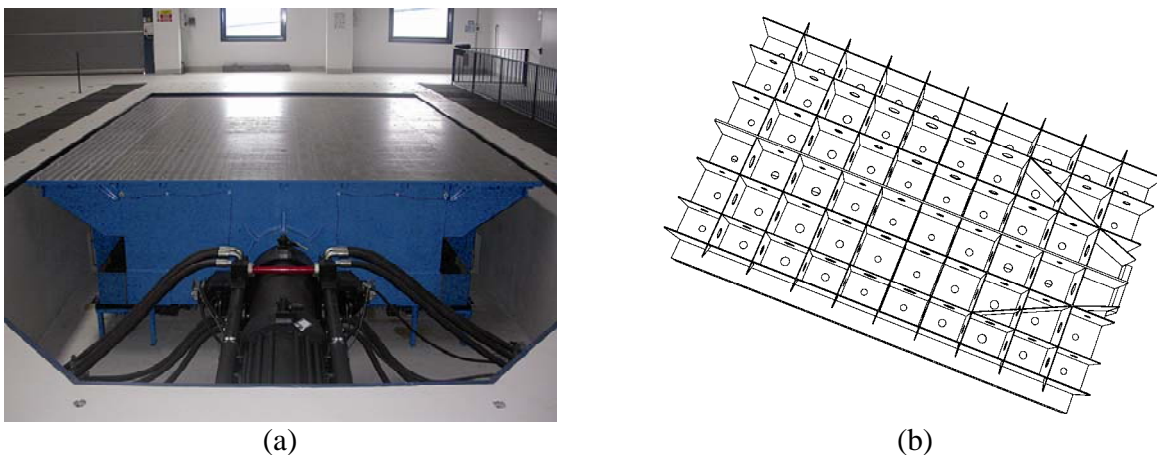


Fig. 1. Shaking table (a) excited by a servo-hydraulic actuator (b) and built as a honey-comb like network of stiffening diaphragms [15]

The dynamic performance of the shaking table system can be significantly affected by potential regions of flexibility [19], e.g., the flexibility of the reaction mass on the suspension system/shock absorbers system; the reaction mass internal flexibility; the axial and lateral bending stiffness of the actuators; the hydraulic oil column bulk modulus stiffness; the axial, torsional and lateral bending stiffnesses of any torsion tubes or other restraining system; and, finally, the flexibility of the platform. The rotational motion of a large dynamic testing facility could be exacerbated by the large overturning moment due to the specimen located on the shaking table (whose interaction with the shaking table dynamics has been studied in [14, 19]). Furthermore, the large lateral displacements and the powerful performance in terms of both velocity and acceleration of the shaking table could emphasise the effects of the interaction between the support system and the shaking table. Finally, the motion of the reaction mass is extremely affected by the deformability of the soil and its dynamic impedance functions and, to the authors' knowledge, this issue has never been taken into account in literature.

All these aspects could cause the presence of non-negligible nonlinear terms in the equations of motion of the dynamic testing facility. These considerations encouraged this research work on the analytical modelling of a large dynamic testing facility in order to account for nonlinear kinematics with the application of the motion composition rules (the velocity composition rule and Coriolis' theorem). Hence, nonlinear equations of motion of the specimen/shaking-table/reaction-mass/isolation-damping-systems/foundation-soil system are derived using the Lagrangian approach, with the assumption of large displacements. It follows that the obtained model is developed for any given uniaxial shaking table whose response could be strongly affected by the possible rocking of the reaction mass. Two methods are followed for the derivation of the analytical model - the energy approach and the direct method of derivation of the equations of motion. Fig. 2 represents a schematic view of the dynamic facility to be analytically modelled. It represents a typical large-scale uniaxial shaking table system where the platform is moved by a servo-hydraulic actuator and the excitation forces are reacted by a large reaction mass, as previously introduced. Two main systems are represented in Fig. 2:

- *System I*, which includes the reaction mass, the springs and the dampers that could represent the stiffness and the damping coefficients of both the isolation system and the surrounding soil,
- *System II*, composed by the shaking table and the specimen (or payload) to be tested.

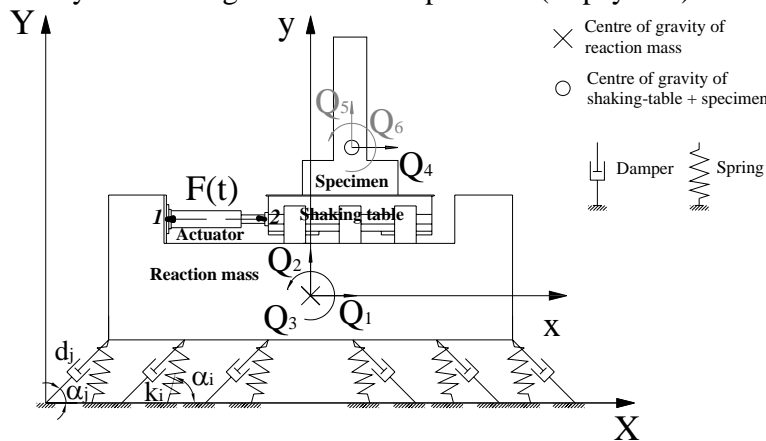


Fig. 2. Schematic view of the large dynamic testing facility to be analytically model

Six generalised coordinates Q_i were initially considered (Fig. 2): three for the *system I* and three for the *system II*. In particular, Q_1 is the absolute displacement along the x - direction, Q_2 is the absolute y -displacement, Q_3 is the absolute rotation in the (x, y) plane, Q_4 is the relative x -displacement, Q_5 is the relative y -displacement, Q_6 is the relative rotation in the (x, y) plane. The displacements Q_1 ,

Q_2 and the rotation Q_3 characterise the motion of *system I*, whereas the displacements Q_4 , Q_5 and the rotation Q_6 represent the relative motion of *system II* with respect to the motion of *system I*. The out-of-plane rotation was not taken into account since a two dimensional model is studied in this formulation phase.

For the sake of simplicity, the first introduced assumption is that the payload is perfectly restrained to the platform and it moves accordingly to the shaking table motion. Therefore, the relative vertical displacement Q_5 and the relative rotation Q_6 are disregarded in this phase of the formulation, whereas the degree of freedom (DOF) Q_3 becomes the rotation of both *system I* and *system II*. Hence, four are the degrees of freedom accounted for the formulation of the nonlinear analytical model (Fig. 2): three generalised coordinates of the centre of gravity of the *system I* – Q_1 , Q_2 , and Q_3 – and only one coordinate for the centre of gravity of the *system II* – Q_4 . Four nonlinear differential equations of motion have to be derived. It is worth noting that the springs and dampers introduced for modelling isolation and damping systems, as well as the impedances of the soil, are not lumped to the centre of gravity of the *system I*. They are distributed along the bottom surface of the reaction mass and could be located with any orientation in the (x, y) frame of reference as it will be explained in the following sections.

2.1. Derivation of the equations of motion using Lagrange's formulation

The Lagrange's equation of motion for a system with n degrees of freedom can be stated as [20]:

$$\frac{d}{dt} \left(\frac{\partial L}{\partial \dot{Q}_i} \right) - \left(\frac{\partial L}{\partial Q_i} \right) + \left(\frac{\partial D}{\partial \dot{Q}_i} \right) = Q_i^* \quad \text{for } i = 1, n \quad (1)$$

where L is the Lagrangian of a system computed as the difference between the total kinetic energy (T) and the total potential energy (V), D is the dissipation function, Q_i the generalised coordinate and \dot{Q}_i its time derivative (i.e., the generalised velocity), and Q_i^* the generalised force applied at the coordinate i . Since $\partial V_i / \partial \dot{Q}_i$ is equal to zero, Eq. (1) can be rewritten as:

$$\frac{d}{dt} \left(\frac{\partial T}{\partial \dot{Q}_i} \right) - \left(\frac{\partial T}{\partial Q_i} \right) + \left(\frac{\partial V}{\partial Q_i} \right) + \left(\frac{\partial D}{\partial \dot{Q}_i} \right) = Q_i^* \quad (2)$$

In the following sections the homogeneous matrix approach proposed by Legnani et al. [21, 22] is applied since it allows the writing of the dynamics equation of a system of rigid bodies following Lagrange's method. This methodology was originally developed to study kinematic and dynamic chains of rigid body systems in the form of a consistent method employing 4x4 matrices. As stated by Legnani [22], the resulting notation is succinct, expressive and convenient for the automatic calculation. In fact, the required position (**M**), velocity (**W**) and acceleration (**H**) matrices allow handling both linear and angular terms at the same time. The dynamic requires the use of the further matrix, usually called pseudo inertial matrix (**J**), describing the mass distribution of the body. The direct application of this methodology is presented in the following sections, where all the ingredients required for writing Eq. (2) are computed after the derivation of the matrices **M**, **W**, **H** and **J** for *system I* and *system II*, respectively. Three frames of reference are used during the formulation: (X_1, Y_1, Z_1) which is the absolute inertial frame of reference; (X_2, Y_2, Z_2) whose origin corresponds to the centre of gravity of the reaction mass (i.e., *system I*); (X_3, Y_3, Z_3) whose origin is located at the centre of gravity of the shaking table-specimen (i.e., *system II*).

2.1.1. Derivation of the kinetic energy T . With reference to Eq. (2), the total kinetic energy T is given by the sum of the kinetic energies of both *system I* (T_I) and *system II* (T_{II}):

$$T = T_I + T_{II} \quad (3)$$

Both energy approach and direct method were employed for the derivation of T , leading to the same final expression. For sake of brevity, only the final results obtained with the energy approach are presented in this section. The expressions of T_I and T_{II} are derived in the reference frame whose origin corresponds to the centre of gravity of *system I*, and expressed as a function of velocity and inertia matrices by means of the trace operator:

$$T_I = (1/2) \cdot \text{Trace}(\mathbf{W}_{12(1)} \mathbf{J}_{I(2)} \mathbf{W}_{12(1)}^T) \quad \text{and} \quad T_{II} = (1/2) \cdot \text{Trace}(\mathbf{W}_{13(1)} \mathbf{J}_{II(1)} \mathbf{W}_{13(1)}^T) \quad (4)$$

where $\mathbf{W}_{12(1)}$ and $\mathbf{W}_{13(1)}$ are the velocity matrices of *system I* and *system II*, respectively, in the reference frame (X_1, Y_1, Z_1) , $\mathbf{J}_{I(2)}$ is the pseudo inertial matrix of *system I* in the reference frame (X_2, Y_2, Z_2) , and $\mathbf{J}_{II(1)}$ is the pseudo inertial matrix of *system II* in the reference frame (X_1, Y_1, Z_1) .

With respect to the frame of reference (X_1, Y_1, Z_1) , the matrices that characterise the motion of *system I* are introduced in Eq. (5). The upper 3×3 sub-matrix of $\mathbf{M}_{12(1)}$ represents the rotational component of motion, whereas the 3×1 vector contains the translational components of motion. With reference to the coefficients of the matrix $\mathbf{H}_{12(1)}$, the second time derivative, \ddot{Q}_3 , represents the real angular acceleration whereas the square of the first time derivative, \dot{Q}_3^2 , is the square of the angular velocity and stands for the *Coriolis' acceleration* that cannot be neglected to correctly describe the motion of a body in a rotating frame element.

$$\mathbf{M}_{12(1)} = \begin{bmatrix} \cos Q_3 & -\sin Q_3 & 0 & Q_1 \\ \sin Q_3 & \cos Q_3 & 0 & Q_2 \\ 0 & 0 & 1 & 0 \\ 0 & 0 & 0 & 1 \end{bmatrix}, \quad \mathbf{W}_{12(1)} = \begin{bmatrix} 0 & -\dot{Q}_3 & 0 & \dot{Q}_1 \\ \dot{Q}_3 & 0 & 0 & \dot{Q}_2 \\ 0 & 0 & 0 & 0 \\ 0 & 0 & 0 & 0 \end{bmatrix}, \quad \mathbf{H}_{12(1)} = \begin{bmatrix} -\dot{Q}_3^2 & -\ddot{Q}_3 & 0 & \ddot{Q}_1 \\ \ddot{Q}_3 & -\dot{Q}_3^2 & 0 & \ddot{Q}_2 \\ 0 & 0 & 0 & 0 \\ 0 & 0 & 0 & 0 \end{bmatrix} \quad (5)$$

The velocity matrix of the *system II* with respect to reference frame (X_1, Y_1, Z_1) is obtained with the following transformations due to *Rivals' theorem* or *velocity composition rule*:

$$\mathbf{W}_{13(1)} = \mathbf{W}_{12(1)} + \mathbf{W}_{23(1)} \quad (6)$$

where $\mathbf{W}_{12(1)}$ is the drag component derived in Eq. (5), while the relative velocity is given by:

$$\mathbf{W}_{23(1)} = \mathbf{M}_{12(1)} \cdot \mathbf{W}_{23(2)} \cdot \mathbf{M}_{21(1)} \quad (7)$$

The velocity matrix $\mathbf{W}_{23(2)}$ as well as the position $\mathbf{M}_{23(2)}$ and acceleration $\mathbf{H}_{23(2)}$ matrices of the *system II* in the frame of reference (X_2, Y_2, Z_2) are obtained as follows:

$$\mathbf{M}_{23(2)} = \begin{bmatrix} 1 & 0 & 0 & Q_4 \\ 0 & 1 & 0 & 0 \\ 0 & 0 & 1 & 0 \\ 0 & 0 & 0 & 1 \end{bmatrix}, \quad \mathbf{W}_{23(2)} = \begin{bmatrix} 0 & 0 & 0 & \dot{Q}_4 \\ 0 & 0 & 0 & 0 \\ 0 & 0 & 0 & 0 \\ 0 & 0 & 0 & 0 \end{bmatrix}, \quad \mathbf{H}_{23(2)} = \begin{bmatrix} 0 & 0 & 0 & \ddot{Q}_4 \\ 0 & 0 & 0 & 0 \\ 0 & 0 & 0 & 0 \\ 0 & 0 & 0 & 0 \end{bmatrix} \quad (8)$$

Therefore, the final expression of the velocity matrix $\mathbf{W}_{13(1)}$ is:

$$\mathbf{W}_{13(1)} = \begin{bmatrix} 0 & -\dot{Q}_3 & 0 & \dot{Q}_1 + \dot{Q}_4 \cos Q_3 \\ \dot{Q}_3 & 0 & 0 & \dot{Q}_2 + \dot{Q}_4 \sin Q_3 \\ 0 & 0 & 0 & 0 \\ 0 & 0 & 0 & 0 \end{bmatrix} \quad (9)$$

The acceleration matrix of the *system II* with respect to the reference frame (X_1, Y_1, Z_1) is obtained by means of the *Coriolis' theorem* that is the *acceleration composition theorem* in the following matrix notation:

$$\mathbf{H}_{13(1)} = \mathbf{H}_{12(1)} + 2 \cdot \mathbf{W}_{12(1)} \cdot \mathbf{W}_{23(1)} + \mathbf{H}_{23(1)} \quad (10)$$

The addenda $\mathbf{H}_{12(1)}$ and $\mathbf{W}_{12(1)}$ are introduced with Eq. (5), $\mathbf{W}_{23(1)}$ is defined in Eq. (7), and finally:

$$\mathbf{H}_{23(1)} = \mathbf{M}_{12(1)} \cdot \mathbf{H}_{23(2)} \cdot \mathbf{M}_{21(1)} \quad (11)$$

After computations, the absolute acceleration $\mathbf{H}_{13(1)}$ is derived as in Eq. (12).

According to Eq. (4), pseudo inertial matrices have to be introduced. The mass distribution of *system I* and *system II* can be represented by symmetric inertial matrices \mathbf{J}_I and \mathbf{J}_{II} , respectively. The pseudo-tensor of inertia of *system I* in the reference frame (X_2, Y_2, Z_2) is written in Eq. (13), on the left, whereas the pseudo-matrix of inertia of the *system II* with respect to the reference frame (X_3, Y_3, Z_3) , whose origin is located in the centre of mass of *system II*, is on the right of Eq. (13).

$$\mathbf{H}_{13(1)} = \begin{bmatrix} -\dot{Q}_3^2 & -\ddot{Q}_3 & 0 & \ddot{Q}_1 - 2\dot{Q}_3\dot{Q}_4 \sin Q_3 + \ddot{Q}_4 \cos Q_3 \\ \ddot{Q}_3 & -\dot{Q}_3^2 & 0 & \ddot{Q}_2 + 2\dot{Q}_3\dot{Q}_4 \cos Q_3 + \ddot{Q}_4 \sin Q_3 \\ 0 & 0 & 0 & 0 \\ 0 & 0 & 0 & 0 \end{bmatrix} \quad (12)$$

$$\mathbf{J}_{I(2)} = \begin{bmatrix} I_{xx,I} & 0 & 0 & 0 \\ 0 & I_{yy,I} & 0 & 0 \\ 0 & 0 & I_{zz,I} & 0 \\ 0 & 0 & 0 & m_I \end{bmatrix} \quad \mathbf{J}_{II(3)} = \begin{bmatrix} I_{xx,II} & 0 & 0 & 0 \\ 0 & I_{yy,II} & 0 & 0 \\ 0 & 0 & I_{zz,II} & 0 \\ 0 & 0 & 0 & m_{II} \end{bmatrix} \quad (13)$$

Using the general transformation law that works for the pseudo-tensor of inertia [22], the mass distribution of the *system II* in the frame of reference (X_1, Y_1, Z_1) is computed with the relationship:

$$\mathbf{J}_{II(1)} = \mathbf{M}_{12(1)} \mathbf{J}_{II(2)} \mathbf{M}_{12(1)}^T = \mathbf{M}_{12(1)} (\mathbf{M}_{23(2)} \mathbf{J}_{II(3)} \mathbf{M}_{23(2)}^T) \mathbf{M}_{12(1)}^T$$

$$\mathbf{J}_{II(1)} = \begin{bmatrix} j_{11(1)II} & j_{12(1)II} & 0 & j_{14(1)II} \\ j_{21(1)II} & j_{22(1)II} & 0 & j_{24(1)II} \\ 0 & 0 & I_{zz,II} & 0 \\ j_{42(1)II} & j_{41(1)II} & 0 & m_{II} \end{bmatrix} \quad (14)$$

where $\mathbf{M}_{23(2)}$ is computed according to Eq. (8) and the remaining addenda are defined as:

$$j_{11(1)II} = (I_{xx,II} + m_{II} Q_4^2) \cos^2 Q_3 + 2m_{II} Q_1 Q_4 \cos Q_3 + I_{yy,II} \sin^2 Q_3 + m_{II} Q_1^2$$

$$j_{22(1)II} = (I_{xx,II} + m_{II} Q_4^2) \sin^2 Q_3 + 2m_{II} Q_2 Q_4 \sin Q_3 + I_{yy,II} \cos^2 Q_3 + m_{II} Q_2^2$$

$$j_{12(1)II} = j_{21(1)II} = (I_{xx,II} + m_{II} Q_4^2) \sin Q_3 \cos Q_3 + m_{II} Q_1 Q_4 \sin Q_3 + m_{II} Q_2 Q_4 \cos Q_3 +$$

$$- I_{yy,II} \sin Q_3 \cos Q_3 + m_I Q_1 Q_2$$

$$j_{14(1)II} = j_{41(1)II} = m_{II} Q_1 + m_{II} Q_4 \cos Q_3$$

$$j_{24(1)II} = j_{42(1)II} = m_{II} Q_2 + m_{II} Q_4 \sin Q_3$$

with m_I and m_{II} masses of *system I* and *system II*, whereas the I_{xx} , I_{yy} , I_{zz} , I_{xy} ($=I_{yx}$), I_{yz} ($=I_{zy}$), I_{xz} ($=I_{zx}$) differ from the usual moments of inertia since they are defined as:

$$I_{xx} = \int x^2 dm \quad I_{yy} = \int y^2 dm \quad I_{zz} = \int z^2 dm \quad I_{xy} = \int xy dm \quad I_{yz} = \int yz dm \quad I_{xz} = \int xz dm \quad (15)$$

Knowing that the trace of a square matrix is the sum of its diagonal elements, the final expression of the kinetic energy T is computed in Eq. (16) where the first row refers to the kinetic energy of the *system I*, and the remaining addenda represent the kinetic energy of the *system II*.

$$T = \begin{cases} (1/2)m_I[\dot{Q}_1^2 + \dot{Q}_2^2] + (1/2)(I_{xx,I} + I_{yy,I})\dot{Q}_3^2 + \\ + (1/2)m_{II}[\dot{Q}_1^2 + \dot{Q}_2^2 + \dot{Q}_4^2 + 2\dot{Q}_1\dot{Q}_4 \cos Q_3 + 2\dot{Q}_2\dot{Q}_4 \sin Q_3] + \\ (1/2)\dot{Q}_3^2[(I_{xx,II} + I_{yy,II}) + m_{II}(Q_1^2 + Q_2^2 + Q_4^2 + 2Q_1Q_4 \cos Q_3 + 2Q_2Q_4 \sin Q_3)] + \\ + m_{II}\dot{Q}_3[Q_1\dot{Q}_2 - Q_2\dot{Q}_1 + (Q_1\dot{Q}_4 - Q_4\dot{Q}_1)\sin Q_3 + (-Q_2\dot{Q}_4 + Q_4\dot{Q}_2)\cos Q_3] \end{cases} \quad (16)$$

2.1.2. *Derivation of the potential energy V.* The total strain energy V is given by several contributions. First of all, the gravity, the potential energies related to the actuator (modelled with a spring whose stiffness is named k_4), the isolation system and the soil (modelled with the introduction of i springs, with stiffness k_i for $i = 1, ns$ where ns is the total number of springs). An additional contribution to V should be the stiffness due to the system of bearings (i.e., guides, actuators, hydrostatic bearings with pressurised oil) that allow the sliding motion of the shaking table. However, in this phase of the formulation, this contribution is not considered. With reference to Fig. 2, the total potential energy is derived after the computations of the following contributions:

$$V = V_P + V_{i_springs} + V_{k4} \quad (17)$$

The addendum V_P represents the potential energy related to the gravitational loads for *system I* and *system II*, respectively:

$$V_P = V_{PI} + V_{PII} \quad \text{with} \quad V_{Pi} = \text{Trace}(-\mathbf{H}_g \cdot \mathbf{J}_i) \quad \text{for } i = I, II \quad (18)$$

where \mathbf{H}_g is the matrix of gravity acceleration whose only non-null component is in y -direction: $-g_y$. For *system I*, the potential energy is computed knowing $\mathbf{J}_{I(1)}$ in the frame of reference (X_1, Y_1, Z_1) . The latter is computed after $\mathbf{J}_{I(2)}$ derived in Eq. (13). Applying the transformation law of this tensor from frame (X_2, Y_2, Z_2) to (X_1, Y_1, Z_1) and the definition of the matrix $\mathbf{M}_{12(1)}$ in Eq. (5), the final expression of this pseudo-tensor of inertia is obtained:

$$\mathbf{J}_{I(1)} = \mathbf{M}_{12(1)}\mathbf{J}_{I(2)}\mathbf{M}_{12(1)}^T = \begin{bmatrix} j_{11(1)I} & j_{12(1)I} & 0 & m_I Q_1 \\ j_{21(1)I} & j_{22(1)I} & 0 & m_I Q_2 \\ 0 & 0 & I_{zz,I} & 0 \\ m_I Q_1 & m_I Q_2 & 0 & m_I \end{bmatrix} \quad (19)$$

with:

$$\begin{aligned} j_{11(1)I} &= I_{xx,I} \cos^2 Q_3 + I_{yy,I} \sin^2 Q_3 + m_I Q_1^2 \\ j_{22(1)I} &= I_{xx,I} \sin^2 Q_3 + I_{yy,I} \cos^2 Q_3 + m_I Q_2^2 \\ j_{12(1)I} &= j_{21(1)I} = I_{xx,I} \sin Q_3 \cos Q_3 - I_{yy,I} \sin Q_3 \cos Q_3 + m_I Q_1 Q_2 \end{aligned}$$

The computation of the potential energy of *system II* requires the knowledge of the tensor $\mathbf{J}_{II(1)}$, already defined in Eq. (14). It follows that, after calculations, the potential energy is obtained as:

$$V_P = g_y m_I Q_2 + g_y [m_{II} Q_4 \sin Q_3 + m_{II} Q_2] \quad (20)$$

With reference to Eq. (17), the elastic potential energy $V_{i_springs}$ must be added to V . The springs could generally represent the stiffnesses of both the isolation system and the soil (Fig. 2). Let \bar{u}_i denote the displacement of the spring whose stiffness is k_i , the potential energy of the ns springs can be simply written as:

$$V_{i_springs} = (1/2) \sum_{i=1}^{ns} k_i \bar{u}_i^2 \quad (21)$$

The displacement \bar{u}_i , which represents the elongation or the shortening of the spring, is determined knowing the old coordinates and the transformation matrix $[T]$ that accounts for the rotation of the

new reference frame with respect to the old one. Since the orientation of each spring is defined by the angle α_i , the displacement \bar{u}_i is given by:

$$\bar{u}_i = [(\cos Q_3 - 1)X_i - \sin Q_3 Y_i + Q_1] \cos \alpha_i + [\sin Q_3 X_i + (\cos Q_3 - 1)Y_i + Q_2] \sin \alpha_i \quad (22)$$

Substituting \bar{u}_i in Eq. (21), the final expression of $V_{i_springs}$ that works for any type of springs, including the ones that represent the stiffness of the soil, is written as follows:

$$V_{i_springs} = (1/2) \sum_{i=1}^{ns} k_i \left\{ [(\cos Q_3 - 1)X_i - \sin Q_3 Y_i + Q_1] (\cos \alpha_i) + [\sin Q_3 X_i + (\cos Q_3 - 1)Y_i + Q_2] (\sin \alpha_i) \right\}^2 \quad (23)$$

The potential energy related to the stiffness of the actuator is calculated as a function of the spring elongation Δl which is the difference between the displacements of two ends of the actuator (i.e., the joints 2 and 1 in Fig. 2):

$$V_{k4} = (1/2) k_4 (\Delta l)^2 = (1/2) k_4 (U_2 - U_1)^2 \quad (24)$$

where k_4 is the translational spring that models the stiffness of the servo-hydraulic actuator. Considering a time interval $(t-t_0)$, the displacements of joint 1 can be computed as the difference between the coordinates of point 1 at time t and t_0 , being the latter the initial time; similarly, for the displacement of joint 2. Since the frame of reference rotates of Q_3 , a transformation matrix must be introduced to compute the coordinates of points 1 and 2 in the rotated frame of reference. After computations, the transformed coordinates U_1 and U_2 of points 1 and 2 are computed as a function of the coordinates (\bar{x}_1, \bar{y}_1) and (\bar{x}_2, \bar{y}_2) of point 1 and 2, respectively, at time t_0 :

$$\begin{aligned} U_1 &= (-\bar{y}_1 Q_3) \cos Q_3 + (\bar{x}_1 Q_3) \sin Q_3 \\ U_2 &= (-\bar{y}_2 Q_3 + Q_4 \cos Q_3) \cos Q_3 + (\bar{x}_2 Q_3 + Q_4 \sin Q_3) \sin Q_3 \end{aligned} \quad (25)$$

Therefore, the potential energy related to spring of stiffness k_4 is given by the following expression:

$$V_{k4} = (1/2) k_4 [Q_4 + \bar{x} Q_3 \sin Q_3 - \bar{y} Q_3 \cos Q_3]^2 \quad (26)$$

where $\bar{x} = \bar{x}_2 - \bar{x}_1$ and $\bar{y} = \bar{y}_2 - \bar{y}_1$. In summary, the total potential energy V is given by the sum of the previously computed contributions of the Eqs. (20), (23) and (26):

$$\begin{aligned} V &= g_y m_I Q_2 + g_y [m_{II} Q_4 \sin Q_3 + m_{II} Q_2] + (1/2) \sum_{i=1}^{ns} k_i \{ [(\cos Q_3 - 1)X_i - \sin Q_3 \cdot Y_i + Q_1] \cdot \\ &\cdot (\cos \alpha_i) + [\sin Q_3 X_i + (\cos Q_3 - 1)Y_i + Q_2] (\sin \alpha_i) \}^2 + (1/2) k_4 [Q_4 + \bar{x} Q_3 \sin Q_3 - \bar{y} Q_3 \cos Q_3]^2 \end{aligned} \quad (27)$$

2.1.3. Derivation of the dissipation function D . Assuming that the dissipated energy is a pseudo-potential energy, it can be introduced into Eq. (2). As stated in Section 2.1.2, the contribution given by the damping of the bearings that allow the sliding motion of the shaking table is not accounted for in this step of the formulation. Therefore, D is computed as the sum of the energy dissipated by the dampers and the actuator (Fig. 2):

$$D = D_{j_dampers} + D_{d4} \quad (28)$$

The general expression of the energy dissipated by the nd external dampers that are immediately beneath the reaction mass and characterized by damping coefficients d_j , is given by:

$$D_{j_dampers} = (1/2) \sum_{j=1}^{nd} d_j \bar{v}_j^2 \quad (29)$$

where \bar{v}_j is the velocity associated to each damper. With reference to Fig. 2, the velocity vector is computed as a function of the horizontal and vertical velocities of *system I* in the absolute frame of

reference, and the angular velocity of both *system I* and *system II*. If α_j is the slope of j -th damper, the velocity becomes equal to:

$$\bar{v}_j = (-\dot{Q}_3 y_j + \dot{Q}_1) \cos \alpha_j + (\dot{Q}_3 x_j + \dot{Q}_2) \sin \alpha_j \quad (30)$$

Therefore, the dissipated function $D_{j_dampers}$ is given by:

$$D_{j_dampers} = (1/2) \sum_{j=1}^{nd} d_j [(-\dot{Q}_3 y_j + \dot{Q}_1) \cos \alpha_j + (\dot{Q}_3 x_j + \dot{Q}_2) \sin \alpha_j]^2 \quad (31)$$

An additional contribution is given by the dissipation factor related to the actuator (Fig. 2):

$$D_{d4} = (1/2) d_4 (\dot{U}_2 - \dot{U}_1)^2 \quad (32)$$

where d_4 is the viscous damping, \dot{U}_2 and \dot{U}_1 are the time-derivatives of the displacements in Eq. (25), representing the velocities of points 2 and 1, respectively. After computations, D_{d4} is equal to:

$$D_{d4} = (1/2) d_4 [\dot{Q}_4 + \bar{x} \dot{Q}_3 (\sin Q_3 + Q_3 \cos Q_3) - \bar{y} \dot{Q}_3 (\cos Q_3 - Q_3 \sin Q_3)]^2 \quad (33)$$

Therefore, the total dissipation function of the dynamic system is derived by:

$$D = (1/2) \sum_{j=1}^{nd} d_j [(-\dot{Q}_3 y_j + \dot{Q}_1) \cos \alpha_j + (\dot{Q}_3 x_j + \dot{Q}_2) \sin \alpha_j]^2 + (1/2) d_4 [\dot{Q}_4 + \bar{x} \dot{Q}_3 (\sin Q_3 + Q_3 \cos Q_3) - \bar{y} \dot{Q}_3 (\cos Q_3 - Q_3 \sin Q_3)]^2 \quad (34)$$

2.1.4. Derivation of the generalised applied force Q_i^* . In this case-study, the applied forces are internal forces due to the servo-hydraulic actuator, along the direction of the actuator (Fig. 2), that is along the degree of freedom Q_4 . Therefore, the force due to the actuator could be defined as a “follower load” which refers to a force applied in a direction tangential to the centre line of the actuator so that it follows the motion of the system as it deforms. If the overall system rotates of Q_3 , the same rotation is suffered by the load applied by the actuator. However, since the applied forces are follower loads, they could not be derived from a potential energy. If the input signal is an acceleration \ddot{u} (i.e., a transient signal, an accelerogram), the Lagrangian force applied to the *system II* is easily calculated as $Q_4^* = |m_{II} \ddot{u}|$. It follows that the components of the Lagrangian forces related to the four considered degrees of freedom are:

$$Q_1^* = -|m_{II} \ddot{u}| \cos Q_3, \quad Q_2^* = |m_{II} \ddot{u}| \sin Q_3, \quad Q_3^* = -|m_{II} \ddot{u}| \cos Q_3 \cdot l, \quad Q_4^* = |m_{II} \ddot{u}| \quad (35)$$

where l is the lever arm between the line of load application and the centre of mass of the *system I*.

2.2. Derived nonlinear differential equations of motion

After the previous computations for deriving the expressions of the kinetic energy T (Section 2.1.1), the potential energy V (Section 2.1.2), the dissipation function D (Section 2.1.3) and, finally, the generalised components of forces Q_i^* (Section 2.1.4), the differential nonlinear equations for describing the motion of the dynamic system are obtained as second-order Lagrange equations, considering four generalized coordinates. Writing Eq. (2) with respect to the coordinate Q_1 , Q_2 , Q_3 and Q_4 , respectively, the four nonlinear differential equations (36)-(39) are obtained. With respect to Q_1 :

$$\begin{aligned} & [m_I \ddot{Q}_1 + m_{II} (\ddot{Q}_1 + \ddot{Q}_4 \cos Q_3 - \dot{Q}_4 \dot{Q}_3 \sin Q_3) - m_{II} \ddot{Q}_3 (Q_2 + Q_4 \sin Q_3) - m_{II} \dot{Q}_3 (\dot{Q}_2 + \dot{Q}_4 \sin Q_3 + \\ & + Q_4 \dot{Q}_3 \cos Q_3)] - \left\{ \dot{Q}_3^2 [m_{II} (Q_1 + Q_4 \cos Q_3)] + m_{II} \dot{Q}_3 [\dot{Q}_2 + \dot{Q}_4 \sin Q_3] + \right. \\ & - \sum_{i=1}^{ns} k_i \{ [Q_1 + x_i (\cos Q_3 - 1) - \sin Q_3 y_i] (\cos \alpha_i)^2 + \sin \alpha_i \cos \alpha_i [\sin Q_3 x_i + (\cos Q_3 - 1) y_i + Q_2] \} \} + \\ & + \sum_{j=1}^{nd} d_j \{ [\dot{Q}_1 - \dot{Q}_3 y_j] (\cos \alpha_j)^2 + [\dot{Q}_2 + \dot{Q}_3 x_j] (\sin \alpha_j \cos \alpha_j) \} = Q_1^* \end{aligned} \quad (36)$$

With respect to Q_2 :

$$\begin{aligned}
& [m_I \ddot{Q}_2 + m_{II} (\ddot{Q}_2 + \ddot{Q}_4 \sin Q_3 + \dot{Q}_4 \dot{Q}_3 \cos Q_3) + m_{II} \ddot{Q}_3 (Q_1 + Q_4 \cos Q_3) + m_{II} \dot{Q}_3 (\dot{Q}_1 + \dot{Q}_4 \cos Q_3 + \\
& - Q_4 \dot{Q}_3 \sin Q_3)] - \left\{ \dot{Q}_3^2 [m_{II} (Q_2 + Q_4 \sin Q_3)] - m_{II} \dot{Q}_3 [\dot{Q}_1 + \dot{Q}_4 \cos Q_3] - [g_y (m_I + m_{II})] + \right. \\
& \left. - \sum_{i=1}^{ns} k_i \{ [Q_2 + x_i \sin Q_3 - (\cos Q_3 - 1) y_i] (\sin \alpha_i)^2 + \sin \alpha_i \cos \alpha_i [(\cos Q_3 - 1) x_i - \sin Q_3 y_i + Q_1] \} \right\} + \\
& + \sum_{j=1}^{nd} d_j \{ [\dot{Q}_2 + \dot{Q}_3 x_j] (\sin \alpha_j)^2 + [\dot{Q}_1 - \dot{Q}_3 y_j] (\sin \alpha_j \cos \alpha_j) \} = Q_2^*
\end{aligned} \tag{37}$$

With respect to Q_3 :

$$\begin{aligned}
& I_I \ddot{Q}_3 + [I_{II} + m_{II} (Q_1^2 + Q_2^2 + Q_4^2 + 2Q_1 Q_4 \cos Q_3 + 2Q_2 Q_4 \sin Q_3)] \ddot{Q}_3 + [2m_{II} (Q_1 \dot{Q}_1 + Q_2 \dot{Q}_2 + Q_4 \dot{Q}_4 + \\
& + \dot{Q}_1 Q_4 \cos Q_3 + Q_1 \dot{Q}_4 \cos Q_3 - Q_1 Q_4 \dot{Q}_3 \sin Q_3 + \dot{Q}_2 Q_4 \sin Q_3 + Q_2 \dot{Q}_4 \sin Q_3 + Q_2 Q_4 \dot{Q}_3 \cos Q_3)] \dot{Q}_3 + \\
& + m_{II} [-Q_1 \ddot{Q}_2 - Q_2 \ddot{Q}_1 + (Q_1 \ddot{Q}_4 - Q_4 \ddot{Q}_1) \sin Q_3 + (Q_1 \dot{Q}_4 - \dot{Q}_1 Q_4) \dot{Q}_3 \cos Q_3 + (\ddot{Q}_2 Q_4 - \ddot{Q}_4 Q_2) \cos Q_3 + \\
& - (Q_4 \dot{Q}_2 - \dot{Q}_4 Q_2) \dot{Q}_3 \sin Q_3] - \left\{ m_{II} (-\dot{Q}_1 \dot{Q}_4 \sin Q_3 + \dot{Q}_2 \dot{Q}_4 \cos Q_3) + \dot{Q}_3^2 [m_{II} (-Q_1 Q_4 \sin Q_3 + \right. \\
& + Q_2 Q_4 \cos Q_3)] + m_{II} \dot{Q}_3 [(Q_1 \dot{Q}_4 - \dot{Q}_1 Q_4) \cos Q_3 - (Q_4 \dot{Q}_2 - \dot{Q}_4 Q_2) \sin Q_3] - [g_y m_{II} Q_4 \cos Q_3] + \\
& \left. - \sum_{i=1}^{ns} k_i \{ [(\cos Q_3 - 1)(-\sin Q_3) x_i^2 + \sin Q_3 \cos Q_3 y_i^2 + (\sin Q_3)^2 x_i y_i + (\cos Q_3 - 1) \cos Q_3 x_i y_i + \right. \\
& \left. - \sin Q_3 x_i Q_1 - \cos Q_3 y_i Q_1] (\cos \alpha_i)^2 + [\sin Q_3 \cos Q_3 x_i^2 + (\cos Q_3 - 1)(-\sin Q_3) y_i^2 + \cos Q_3 \cdot \right. \\
& \cdot (\cos Q_3 - 1) x_i y_i + (\sin Q_3)^2 x_i y_i + \cos Q_3 x_i Q_2 - \sin Q_3 y_i Q_2] (\sin \alpha_i)^2 + [(\sin Q_3)^2 x_i^2 + (\cos Q_3 - 1) \cdot \\
& \cdot \cos Q_3 x_i^2 + 2(\cos Q_3 - 1)(-\sin Q_3) x_i y_i - \sin Q_3 Q_2 x_i - 2 \sin Q_3 \cos Q_3 x_i y_i - \cos Q_3 (\cos Q_3 - 1) y_i^2 + \\
& \left. + (\sin Q_3)^2 y_i^2 - Q_2 \cos Q_3 y_i + Q_1 \cos Q_3 x_i + Q_1 (-\sin Q_3) y_i] (\sin \alpha_i \cos \alpha_i) \right\} + \\
& + k_4 [Q_4 + \bar{x} Q_3 \sin Q_3 - \bar{y} Q_3 \cos Q_3] \cdot [\bar{x} (\sin Q_3 + Q_3 \cdot \cos Q_3) - \bar{y} (\cos Q_3 - Q_3 \sin Q_3)] + \\
& + \sum_{j=1}^{nd} d_j \{ [\dot{Q}_3 y_j^2 - \dot{Q}_1 y_j] (\cos \alpha_j)^2 + [\dot{Q}_3 x_j^2 + \dot{Q}_2 x_j] (\sin \alpha_j)^2 + [\dot{Q}_1 x_j - \dot{Q}_2 y_j - 2\dot{Q}_3 x_j y_j] \cdot \\
& \cdot (\sin \alpha_j \cos \alpha_j) \} + d_4 [\dot{Q}_4 + \bar{x} \dot{Q}_3 (\sin Q_3 + Q_3 \cos Q_3) - \bar{y} \dot{Q}_3 (\cos Q_3 - Q_3 \sin Q_3)] \cdot \\
& \cdot [\bar{x} (\sin Q_3 + Q_3 \cdot \cos Q_3) - \bar{y} (\cos Q_3 - Q_3 \cdot \sin Q_3)] = Q_3^*
\end{aligned} \tag{38}$$

With respect to Q_4 :

$$\begin{aligned}
& [m_{II} (\ddot{Q}_4 + \ddot{Q}_1 \cos Q_3 + \ddot{Q}_2 \sin Q_3 - \dot{Q}_1 \dot{Q}_3 \sin Q_3 + \dot{Q}_2 \dot{Q}_3 \cos Q_3) + m_{II} \ddot{Q}_3 (Q_1 \sin Q_3 - Q_2 \cos Q_3) + \\
& + m_{II} \dot{Q}_3 (\dot{Q}_1 \sin Q_3 + Q_1 \dot{Q}_3 \cos Q_3 - \dot{Q}_2 \cos Q_3 + Q_2 \dot{Q}_3 \sin Q_3)] - \left\{ \dot{Q}_3^2 [m_{II} (Q_4 + Q_1 \cos Q_3 + \right. \\
& + Q_2 \sin Q_3)] + m_{II} \dot{Q}_3 [-\dot{Q}_1 \sin Q_3 + \dot{Q}_2 \cos Q_3] - g_y m_{II} \sin Q_3 - k_4 [Q_4 + \bar{x} Q_3 \sin Q_3 + \\
& \left. - \bar{y} Q_3 \cos Q_3] \right\} + d_4 [\dot{Q}_4 + \bar{x} \dot{Q}_3 (\sin Q_3 + Q_3 \cos Q_3) - \bar{y} \dot{Q}_3 (\cos Q_3 - Q_3 \sin Q_3)] = Q_4^*
\end{aligned} \tag{39}$$

With reference to Fig. 2, the symbols used in the four equations are defined as follows:

- m_I is the mass of the reaction mass (*system I*);
- m_{II} is the mass of the shaking table and the test specimen, if any (*system II*);
- $I_I = I_{xx,I} + I_{yy,I}$ and $I_{II} = I_{xx,II} + I_{yy,II}$
- g_y is the gravity acceleration;
- x_i, y_i, α_i are the coordinates and the slope of the i -th spring;
- x_j, y_j, α_j are the coordinates and the slope of the j -th damper;
- k_4, d_4 are the stiffness and the damping of the servo-hydraulic actuator;
- $\bar{x} = \bar{x}_2 - \bar{x}_1$ and $\bar{y} = \bar{y}_2 - \bar{y}_1$, where 1 and 2 refer to the ends of the servo-hydraulic actuator.

Eqs. (36)-(39) form a complete system of differential equations describing the motion of a large dynamic testing facility designed for performing single-axis tests but that could be affected by

possible large rotations. The solution strategies and some of the preliminary verifications of the developed analytical model, as well as the comparisons with the experimental data of a real case-study are presented in the following sections.

3. PRELIMINARY VERIFICATIONS

An additional aim of this study is the computation of the solutions of the above nonlinear differential equations. There are two ways for solving the dynamic equations of a system model [16]. For a quick and approximate solution, linear analysis techniques can be used. The resulting approximations of system response provide insight into why the solution has certain features and how the system might be changed to modify the response in a desired direction. In contrast, a precise picture of the system response typically calls for numerical techniques to solve the system equations.

To facilitate and systematise the solution of ordinary constant-coefficient differential equations, the Laplace-transform method is used extensively [17]. However, to the authors' knowledge, the nonlinearity of the equations is not explicitly dealt with Laplace transforms. Therefore, the solutions of the Eqs. (36)-(39) could be found with the Laplace transforms only after a linearization of the problem. Since the nonlinearity of the dynamic model cannot be neglected, numerical solution methods, capable of solving linear as well as nonlinear differential equations, have been investigated. For numerically solving the derived differential equations of Section 2.2, the fourth order Runge-Kutta methods are employed ("ode45" solver in Matlab [23]) because of their good efficiency. They provide solutions which are comparable in accuracy to Taylor series solution in which higher order derivatives are retained. Higher order differential equations can be treated as if they were a set of first-order equations. These methods allow one to vary the step size and use only initial values.

However, before solving the four differential nonlinear equations of motion (36)-(39), some well-known results are derived after the introduction of assumptions that simplify or "linearise" them. If well-known results can be derived from very complex systems of equations, this could be considered as a first proof of the accuracy of the model itself. In the next section, some of the linearised models derived from Eqs. (36)-(39) are introduced. Moreover, the verification of the accuracy of both the equations and the numerical solver is discussed in Section 3.2. Then a comparison with a lumped mass model used in the design phase of an existing large-scale dynamic testing facility is presented (Section 3.3).

3.1. Some "linearisation" of the derived nonlinear equations of motion

As mentioned above, it is useful to linearise models in order to compare results with those of well-known systems. In the next paragraphs, only two of the derived linearised models for representative systems are introduced.

a) *System with two degrees of freedom – Q_1 and Q_4 .* The first considered configuration is characterized by a rotation Q_3 equal to zero. The second introduced assumption is that the total strain energy V and the dissipation function D are nil. Therefore, the previously derived Lagrangian assumes the following expression in (40). After the assumptions of free-body conditions, the equation of motion (41) for the horizontal translation represents the first well-known outcome:

$$L = T - V = T|_{Q_3=0} = (1/2)m_I(\dot{Q}_1^2 + \dot{Q}_2^2) + (1/2)m_{II}(\dot{Q}_1^2 + \dot{Q}_2^2 + \dot{Q}_4^2 + 2\dot{Q}_1\dot{Q}_4) \quad (40)$$

$$\ddot{Q}_1 = \frac{-m_{II}}{(m_I + m_{II})}\ddot{Q}_4 = -\frac{m_{II}}{m_{tot}}\ddot{Q}_4 = \frac{-1}{(m_I/m_{II} + 1)}\ddot{Q}_4 \quad (41)$$

It results that the generalized acceleration \ddot{Q}_1 of the *system I* approaches to zero if the total mass m_{tot} approaches to infinity, or even if $m_I \gg m_{II}$. This implies that the acceleration of the reaction mass system decreases increasing its mass (m_I) with respect to the movable mass of shaking table-specimen system (m_{II}). This result is intuitive and well-known in literature, and justifies the fact that the reaction mass should be typically 30 to 50 times the specimen-shaking table mass, as stated by Clark [18]. This advice has been followed in the majority of the designs of the existing shaking tables [15] in order to reduce as much as possible the motion of the reaction mass, due to the motion transmitted by the shaking table.

b) *System with two degrees of freedom – Q_4 and Q_3* . The second configuration is derived from the Eqs. (36)-(39), setting the generalized translational coordinates of the reaction mass (Q_1, Q_2) equal to zero and, consequently, the corresponding velocities. In Fig. 3 are compared two cases of study for verifying the accuracy of the analytical model. The obtained equations of motion represent the well-known equations of classical mechanics [20] describing the motion of a lumped mass restrained to slide along a rod (that is, a predefined direction) which rotates around its centre of gravity with rotational velocity \dot{Q}_3 . The first set of equations is derived for the simple model in Fig. 3(a) and compared with the one obtained with a direct formulation by Goldstein [20], leading to the same final results.

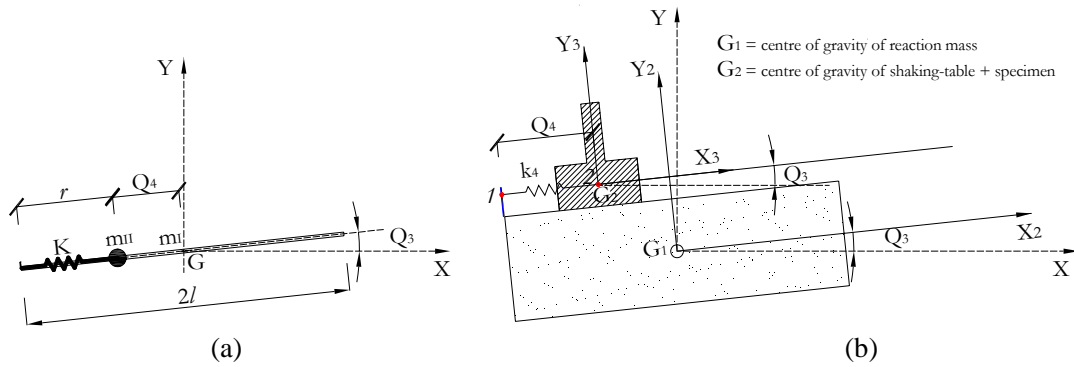


Fig. 3. Comparisons of two cases of study: (a) a lumped mass m_{II} restrained to slide along a rod which rotates around its centre of gravity, and (b) the dynamic system with two DOFs – Q_4 and Q_3 .

Then, the model in Fig. 3(b) is studied, with k_4 representing the stiffness of the servo-hydraulic actuator along the sliding direction of the movable mass m_{II} - as the spring K in Fig. 3(a). The derived equations of motion are:

$$\begin{cases} m_{II}\ddot{Q}_4 - m_{II}Q_4\dot{Q}_3^2 + k_4(l - Q_4) = 0 \\ [(I_{xx,I} + I_{yy,I}) + (I_{xx,II} + I_{yy,II} + m_{II}Q_4^2)]\ddot{Q}_3 + 2m_{II}Q_4\dot{Q}_3\dot{Q}_4 = 0 \end{cases} \quad (42)$$

These equations are similar to the ones describing the motion of the model in Fig. 3(a), and, hence, to the expressions of classical mechanics [20]. This represents a proof of the accuracy of the derived analytical model. Finally, it has to be pointed out that the studied system, even if very simple, reveals a significant interaction between the considered degrees of freedom since the rotation Q_3 could affect the sliding motion Q_4 with non-negligible effects, and vice-versa.

3.2. Verification of the accuracy of both the equations of motion and the numerical solver

The verification of the accuracy of the Eqs. (36)-(39) is firstly carried out applying the following mathematical procedure. Known and simple solutions are imposed to the equations of motion, and the forces satisfying the equilibrium are derived. These forces become the external loads to be applied to the system of equations and the corresponding solutions are calculated. If the latter are

comparable with the initially imposed solutions within an acceptable tolerance, this is a proof that the equations of motion are accurate and that the numerical solver works properly.

The first step is the writing of the Eqs. (36)-(39) in a canonical form as follows:

$$A_k \cdot \ddot{Q}_1 + B_k \cdot \ddot{Q}_2 + C_k \cdot \ddot{Q}_3 + D_k \cdot \ddot{Q}_4 - E_k = 0 \text{ for } k = 1, 2, 3, 4 \quad (43)$$

In order to apply the Runge-Kutta method, eight new variables are introduced:

$$\begin{aligned} y_1 = Q_1, \quad y_2 = \dot{Q}_1, \quad y_3 = Q_2, \quad y_4 = \dot{Q}_2, \quad y_5 = Q_3, \quad y_6 = \dot{Q}_3, \quad y_7 = Q_4, \quad y_8 = \dot{Q}_4 \\ \rightarrow \dot{y}_2 = \ddot{Q}_1, \quad \dot{y}_4 = \ddot{Q}_2, \quad \dot{y}_6 = \ddot{Q}_3, \quad \dot{y}_8 = \ddot{Q}_4 \end{aligned} \quad (44)$$

Therefore, eight first-order nonlinear differential equations of motion are derived. It is worth noting that the distribution and the pose (Fig. 2) of the springs k_i ($i = 1, ns$) and the dampers d_j ($j = 1, nd$) are explicitly taken into account in the computations since this is one of the main features of the proposed dynamic model. The validation of the accuracy of the equations performed in this section is based on a numerical example where only horizontal and vertical springs are taken into account (i.e. $\alpha_i = 0^\circ$ and $\alpha_i = 90^\circ$, respectively); similarly for the dampers (i.e. $\alpha_j = 0^\circ$ and $\alpha_j = 90^\circ$, respectively). Applying these assumptions into Eq. (43) and using the Gauss elimination method, the new set of eight differential equations can be solved by Runge-Kutta method. Following the steps of the introduced mathematical procedure, simple solutions are applied to the equations of motion, such as the ones in (45) with the initial conditions in (46):

$$Q_1(t) = Q_{1o} \cos(\omega_s t), \quad Q_2(t) = Q_{2o} \cos(\omega_s t), \quad Q_3(t) = Q_{3o} \cos(\omega_s t), \quad Q_4(t) = Q_{4o} \cos(\omega_s t) \quad (45)$$

$$\{y_1(0), y_2(0), y_3(0), y_4(0), y_5(0), y_6(0), y_7(0), y_8(0)\}^T = \{Q_{1o}, 0, Q_{2o}, 0, Q_{3o}, 0, Q_{4o}, 0\}^T \quad (46)$$

Solving the dynamic model with the imposed solutions (45), the four expressions of the loads - \bar{F}_{Q1} , \bar{F}_{Q2} , \bar{M}_{Q3} and \bar{F}_{Q4} - are computed. The latter are then applied as external forces leading to a new set of solutions to be compared with the ones in Eq. (45). The results plotted in Fig. 4 are obtained with the data of one of the numerical examples carried out during the verification procedure. The plots show very good agreement between the imposed and computed solutions. The high quality of the results is due to the application of the error tolerance properties (according to [23]).

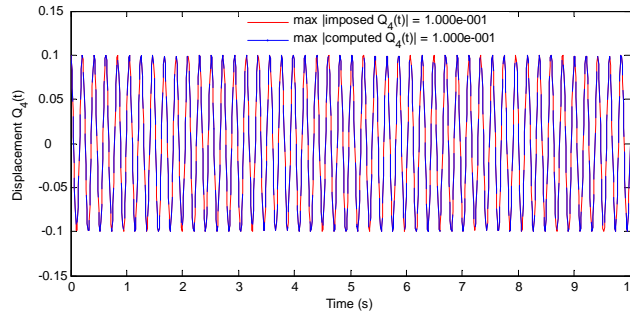


Fig. 4. Comparison between the imposed and computed solutions of a numerical example solving Eq. (43). Plot of the displacement Q_4 that is one of the four solutions

During the numerical verifications, the influence of the time step on the accuracy of the numerical solver has been studied imposing simple external loads (e.g. harmonic forces) and solving Eq. (43) with the time step as parameter. In fact, regardless of the integration technique, the time step remains an important determinant of when to compute the solutions, and when to compare the model to data. It was derived that the time step cannot be uniquely defined since, for each analysis, it has to be selected as the one that provides more accuracy with less increase in the computing time.

3.3. Comparison with a lumped model used in the design phase of an existing large-scale dynamic testing facility

During the preliminary verifications of the analytical model, a comparison with the numerical simulations carried out for designing an existing large-scale dynamic testing facility is performed. The case-study refers to the large uniaxial shake table built in the laboratory of EUCENTRE (European Centre for Training and Research in Earthquake Engineering), in Italy. The latter has been chosen for its large dimensions (5.6 m by 7.0 m) and powerful characteristics in terms of displacement (peak values ± 0.5 m), velocity (peak values ± 1.5 m/s) and acceleration (peak value 1.8 g with a maximum specimen mass of 60 tonnes) applicable to the test-specimen (with a maximum overturning moment capacity of 4000 kNm that is 1000 kN at 4 m from the top plate of the platform). An exhaustive description of this dynamic testing facility is given in [15].

During the design phase of the facility, the study of the dynamic soil-structure interaction was performed in order to predict the ground motion induced by the excitation of the shaking table. For this reason, a simplified analytical model of the reaction-mass/foundation was developed for estimating the motion transmitted to the soil. A linear lumped mass model was formulated with two degrees of freedom (i.e. Q_1 and Q_3), under the assumptions of small displacements and small rotations. The dynamic impedance functions characterising the soil were defined applying unit harmonic non-quadratic loads to all DOFs within the possible operational frequency range (0÷20 Hz) of the dynamic testing facility (Table 1). The lumped mass model was analysed applying random excitation signals with the criterion of reproducing the excitation that should be used in running the experimental tests with the shaking table. The solutions (i.e., displacement and rotation) were computed in frequency domain, with frequency dependent damping and stiffness coefficients and without the possibility of taking into account the initial conditions since the Fourier transforms (FT) were employed. Then, the obtained solutions were converted back in time domain with the inverse transforms and the velocities and accelerations were calculated from the time-histories of the solutions using central difference method [24]. The amplification of accelerations and displacements transmitted to the reaction-mass/foundation/soil corresponding to the isolator resonance frequency led to discarding any type of isolation device (i.e., the airbags). Neither base isolation nor damping systems were designed to mitigate the vibration impact induced by the experimental simulations.

The results of the numerical simulations performed during the design phase are compared in this section with the solutions of a linearised model derived from the complete set of nonlinear second-order differential Eqs. (36)-(39). The comparison has been carried out in terms of accuracy, required input data and time-consuming of the performed analyses. The equations corresponding to the ones used during the design phase of the EUCENTRE shaking table are obtained from Eqs. (36)-(39) after some simplifying assumptions, that is both the coordinate Q_4 and the mass m_{II} are ignored, the springs and the dashpots are lumped in the centre of gravity of *system I*, the rotation Q_3 is small (that is $Q_3 \approx 0$, $\sin Q_3 \approx Q_3$ and $\cos Q_3 \approx 1$), and the DOF Q_2 can be disregarded since it has no interaction with the horizontal and vertical coordinates, leading to:

$$\begin{cases} m_I \ddot{Q}_1 + c_{11} \dot{Q}_1 + c_{13} \dot{Q}_3 + k_{11} Q_1 + k_{13} Q_3 = F_{Q1} \\ (I_{xx,I} + I_{yy,I}) \ddot{Q}_3 + c_{31} \dot{Q}_1 + c_{33} \dot{Q}_3 + k_{31} Q_1 + k_{33} Q_3 = M_{Q3} \end{cases} \quad (47)$$

These linearised equations correspond to the governing equations of the linear model used during the design phase of the EUCENTRE shaking table [15], in what follows named “linear design model” and compared with the “linearised proposed model” of Eq. (47). The coefficients c_{ij} and k_{ij} represent the damping and stiffness coefficients (i.e., the impedance functions) of the soil. It is worth noting that, in the design model, they were computed as frequency dependent (Table 1).

Since Eq. (47) is directly solved in the time domain using the Runge-Kutta method (RK), it is not possible to introduce frequency dependent coefficients. Therefore, with reference to the impedance functions derived for the linear design model, “average” values for c_{ij} and k_{ij} are selected such that the equal energy concept is saved (Table 1). Introducing four new variables y_1, y_2, y_3 and y_4 in Eq. (47), the following four first order differential equations are derived and solved with nil initial conditions, as it was assumed during the numerical simulations of the design phase:

$$\begin{cases} \dot{y}_1 = y_2 \\ \dot{y}_2 = [F_{Q1} - (c_{11} \cdot y_2 + c_{13} \cdot y_4 + k_{11} \cdot y_1 + k_{13} \cdot y_3)]/m_I \\ \dot{y}_3 = y_4 \\ \dot{y}_4 = [M_{Q3} - (c_{31} \cdot y_2 + c_{33} \cdot y_4 + k_{31} \cdot y_1 + k_{33} \cdot y_3)]/(I_{xx,I} + I_{yy,I}) \end{cases} \quad (48)$$

For comparison with the results presented in [15], the external force F_{Q1} and overturning moment M_{Q3} are derived from the analyses of a reinforced concrete (RC) column subjected to several ground motions. For the geometrical data and reinforcement details of the full-scale bridge piers, the reader is referred to [25]. Some of the numerical responses computed solving Eqs. (47) are plotted in Fig. 5 (Q1_{RK} and Q3_{RK}), considering the excitation action time-histories due to Coalinga record. These solutions have to be compared with the results of the linear design model and plotted in Fig. 5 (Q1_{FT} and Q3_{FT}). In the compared numerical simulations, the reaction mass weights 2178 tonnes, and F_{Q1} and M_{Q3} reach the peak values of 980.2 kN and 5301 kN m, respectively.

It is worth noting that the time-histories of the responses called Q1_{RK} and Q3_{RK} in Fig. 5 are the solutions of the linearised proposed model and are directly obtained in time-domain with “average” values for both the stiffness and damping coefficients of the soil (Table 1). However, this assumption does not reduce the accuracy of the obtained results when compared with the solutions of the design model solved in frequency domain considering frequency dependent soil impedances (Table 1). Even in terms of computing time for performing the analyses, the adopted numerical solver (RK) is faster than the application of Fourier Transforms. Therefore, it can be stated that the solutions computed from the linearised proposed model agree well with the ones obtained during the design phase of the EUCENTRE shaking table.

Table 1. Comparisons of the stiffness and damping constants of the soil adopted in the linear design model and in the linearised proposed model, respectively

Design Model	k_{11} (kN/m)	k_{13} (kN/m)	k_{33} (kN/rad)	c_{11} (kN/m)	c_{13} (kN/rad/s)	c_{33} (kNm/rad/s)
0 Hz	3.82×10^6	-5.95×10^6	2.65×10^8	7.25×10^5	-11.03×10^5	3.95×10^7
÷	÷	÷	÷	÷	÷	÷
20 Hz	2.69×10^6	-2.63×10^6	1.72×10^8	7.41×10^4	-0.57×10^5	2.91×10^6
Proposed Model	$k_{11 \text{ avg}}$	$k_{13 \text{ avg}}$	$k_{33 \text{ avg}}$	$c_{11 \text{ avg}}$	$c_{13 \text{ avg}}$	$c_{33 \text{ avg}}$
	4.15×10^6	-4.31×10^6	2.08×10^8	9.87×10^4	-0.56×10^5	2.72×10^6

This step represents a further proof of the accuracy of both the proposed analytical model and the applied numerical solver. In fact, this section presents the comparison of the numerical responses computed with two completely different models (linear design model versus linearised proposed model) and solved with two very different solving techniques (FT versus RK methods).

In this section the model, proposed for describing the behavior of a shaking table designed to perform single-axis tests, and extended to take into account the effects of nonlinear kinematics due to possible rotations, has been preliminarily validated through the comparison with simple available numerical tests carried out considering an existing shaking table. This comparison shows that the proposed model can reproduce the results of simple available examples after a linearization process and some simplifying assumptions.

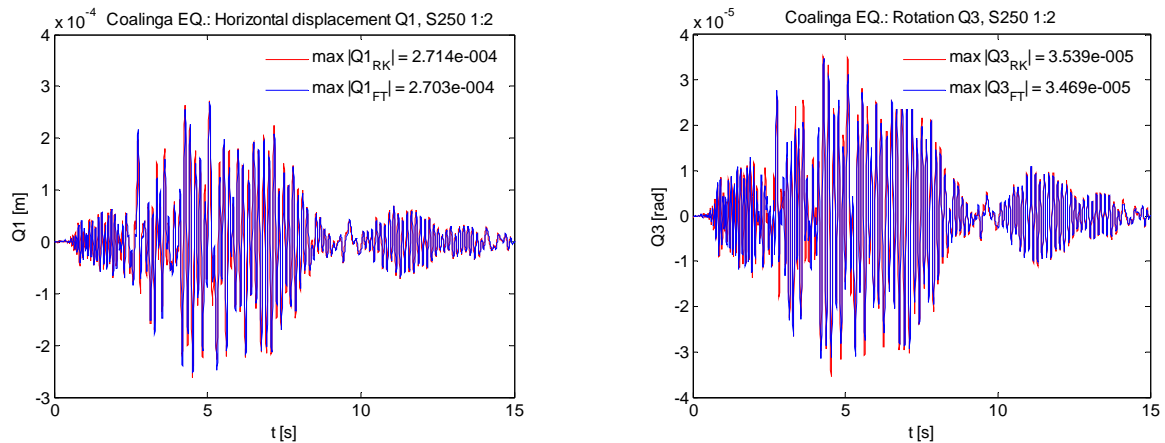


Fig. 5. Translational displacement Q_1 and rotation Q_3 of the centre of mass of the reaction mass block, obtained with the linearised proposed model ($Q_{i_{RK}}$) vs the linear design model ($Q_{i_{FT}}$), under Coalinga record

4.APPLICATION TO A REAL CASE-STUDY

As described in the previous sections, the developed analytical model is formulated to be applicable to any large-scale dynamic testing facility that moves in the longitudinal direction. However, an analytical model should be always verified against experimental data, whenever feasible. Therefore, this section is devoted to the preliminary validation of the developed analytical model with data recorded during real tests of the EUCENTRE shaking table.

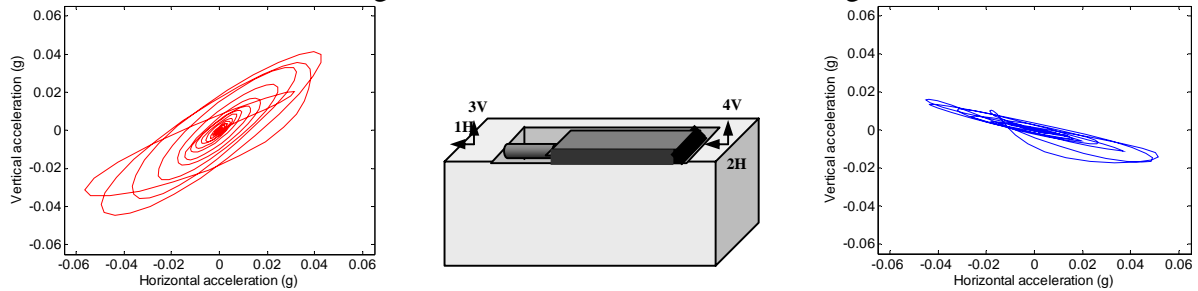


Fig. 6. Compositions of the measured acceleration components at the two sides of the reaction mass – 1H vs 3V (at the actuator side) on the left, 2H vs 4V (at the opposite side) on the right

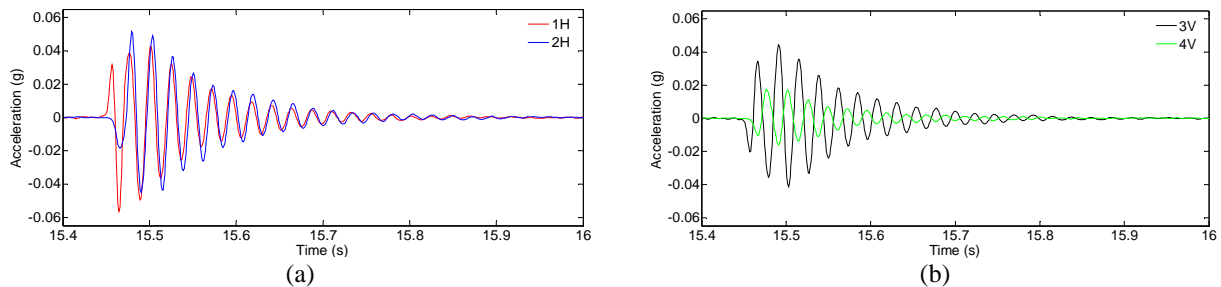


Fig. 7. Comparison of the measured (a) horizontal and (b) vertical responses at the opposite sides of the reaction mass of the EUCENTRE shaking table

As previously introduced, the latter was chosen for its large dimensions and powerful characteristics. In addition, the reaction-mass/shaking-table/specimen system constitutes a non-equilibrated structure due to the eccentric position of both the platform and the test specimen. The former is eccentric with respect to the centre of gravity of the reaction mass, the latter for its own configuration. Therefore, this system could suffer rotation and could be characterised by a

nonlinear response if large rotations are activated during an experimental test. Finally, it has been observed that the reaction mass suffered a rigid rotation probably due to the settlement of the system [26]. This rotation could have a non negligible effect on the response of the dynamic facility since it represents an initial condition that is a transient vibration [24].

Fig. 6 and Fig. 7 show the rocking of the dynamic testing facility due to the sudden stop while retracting the actuator and then free vibration. This response was measured during the experimental campaign described in [27]: the test was performed at both low-magnitude excitation and bare-table condition; therefore, this response is not affected by the specimen's overturning.

It is worth noting that all the aspects previously discussed are taken into account in the proposed formulation. Before presenting the application of the developed nonlinear dynamic model to a real-case study, a brief description of the available experimental tests is given in order to clarify the main steps that characterised this validation phase.

4.1. Available experimental results

Two are the experimental tests available for this second preliminary validation. They were performed during the calibration phase of the EUCENTRE dynamic testing facility in order to analyse the actual behaviour of the shaking table and to verify the assumptions carried out in the design process (Section 3.3). The complete description of the test campaign can be found in [27]. The location and the names assigned to the different instruments of these experiments are shown in Fig. 8. During these two tests, a rigid payload of 60 tonnes, composed by a layer of RC cubic elements with 2.4 m side, was located on the shaking table (therefore, a rigid mass of 60 tonnes is applied at 1.2 m from the top plate of the platform). Table 1 summarises the type of signal and the instrumentation of the experiments. As stated in [27], the input motion used during these two tests was the Coalinga record at 100% magnitude.

Table 1. Available tests carried out at the EUCENTRE Laboratory, from [27]

<i>Test</i>	<i>Type of signal</i>	<i>Instrumentation</i>
N° 1 (21/09/2005)	Coalinga record at 100% magnitude	1 geophone located on the reaction mass in the zone of the actuator anchorage.
N° 2 (30/09/2005)	Coalinga record at 100% magnitude	1 geophone located on the centre right hand side of the reaction mass and 8 servo-accelerometers located at the borders and edges of the reaction block.

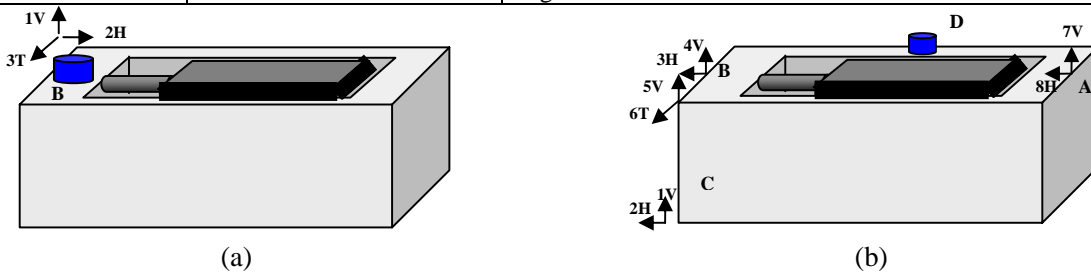


Fig. 8. Distributions of the instrumentations during the application of Coalinga record for Test (a) N° 1 and (b) N° 2, as described in Table 1

In Fig. 9(a) are plotted the vertical and horizontal velocities recorded by the geophone located as in Fig. 8(a). It should be noted that the amplitude of the vertical velocity is half of that of the horizontal component. During Test N° 1, no geophone was put on the right side of the reaction mass, opposed to the actuator side, in order to measure, simultaneously, the velocities at both ends. Therefore, a proof of the possible rocking that could affect the response of the dynamic facility cannot be derived from the signals acquired during this test.

During Test N° 2, a 3D geophone was placed at the centre part of the reaction mass, at location D in Fig. 8(b), and the recorded velocities are plotted in Fig. 9(b). Comparing the horizontal and vertical components of Fig. 9(b) with the ones in Fig. 9(a), it should be apparent that the amplitudes are extremely different. This could be due to the attenuation of both the horizontal and vertical motion moving from the actuator anchorage side to the centre part of the reaction mass.

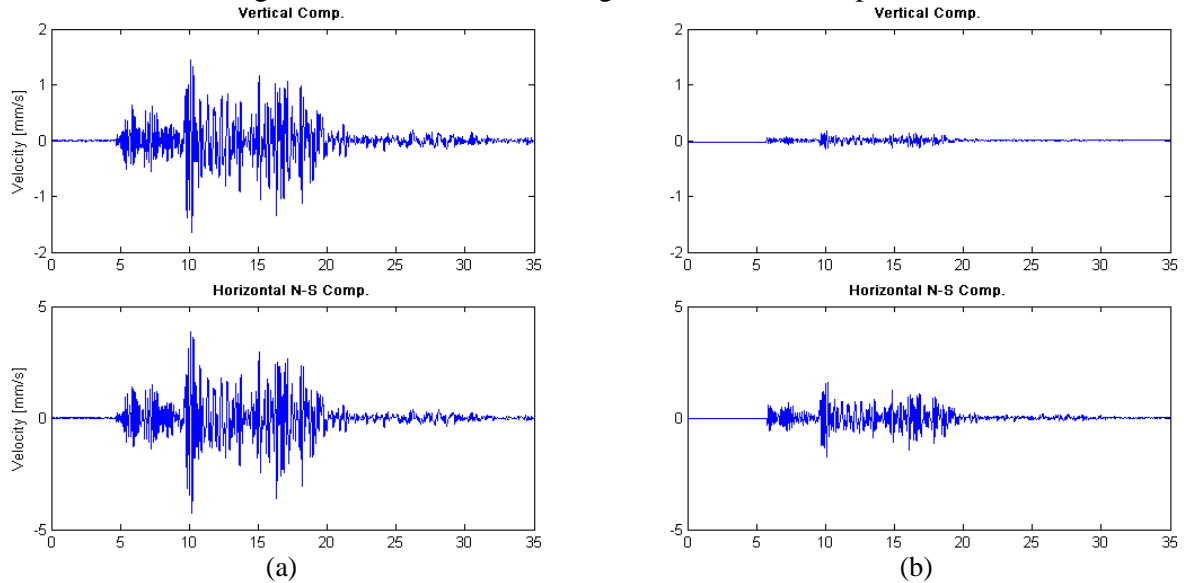


Fig. 9. Velocities recorded by the geophone (a) at the actuator side (Fig. 8a) and (b) at the centre part of the reaction mass (Fig. 8b)

The other available experimental data from Test N° 2 are the accelerations acquired by the servo-accelerometers (1V-8H in Fig. 8b). Fig. 10 presents the time histories of the vertical and horizontal components in three main locations of the reaction mass according to the name convention introduced in Fig. 8: the label “down” refers to the signals measured at location C, “up-actuator” at location B, and “up-opposed” at location A. These plots show that there is a large difference in the attenuation of the signals at the two sides of the reaction mass, reaching lower values at the opposite side of the actuator anchorage zone – “up-actuator” versus “up-opposed”. The same conclusion could be applied comparing the signals recorded at the same side of the reaction mass – “up-actuator” versus “down”.

It was claimed in [27] and reported in Table 1 that the applied input signal was the Coalinga record for both experiments. However, there is a non negligible difference between the velocities of Test N° 1 with those acquired during Test N° 2, mainly in terms of frequency content. Moreover, from a comparison between the time-histories of the velocities (Fig. 9) and the accelerations (Fig. 10), it could be apparent that there is no clear correlation between them. Furthermore, since the real signal applied during these tests is not available, there is some uncertainty related to the application of the same input signal during Tests N°1 and 2.

The experimental results previously plotted from Fig. 9 to Fig. 10 reveal that the response of the reaction mass due to Coalinga record at 100% magnitude is different from the behaviour observed in Fig. 6 and Fig. 7, mainly in terms of the attenuation of the motion.

Since the signals recorded from the geophone seem much more reliable than the ones measured from the servo-accelerometers, they become the main reference for the comparison with the results obtained from the proposed dynamic model, as described in the following section.

4.2. Numerical results

Considering the experimental responses previously plotted, it results that the motion of the reaction block is complex and affected by rocking. Therefore, this could suggest that the distribution of the stiffness and damping coefficients of the soil is not uniform in the longitudinal direction, that is the direction of both the force application and the allowed motion of the shaking table. For this reason, the observed motion could not be reproduced (and predicted) with an analytical model with lumped springs and dashpots like the one used during the design phase of the dynamic testing facility (described in Section 3.3). It has to be used an analytical model that accounts for springs and dashpots distributed, in a non-uniform manner, along the base of the reaction mass.

As described in Section 2, the developed formulation accounts for ns springs, nd dashpots located along the reaction mass base, each one with different values of stiffness k_i and damping d_j , and also with different poses α_i and α_j , respectively. Hence, the observed non-uniform distribution of both stiffness and damping can be reproduced with the proposed dynamic model.

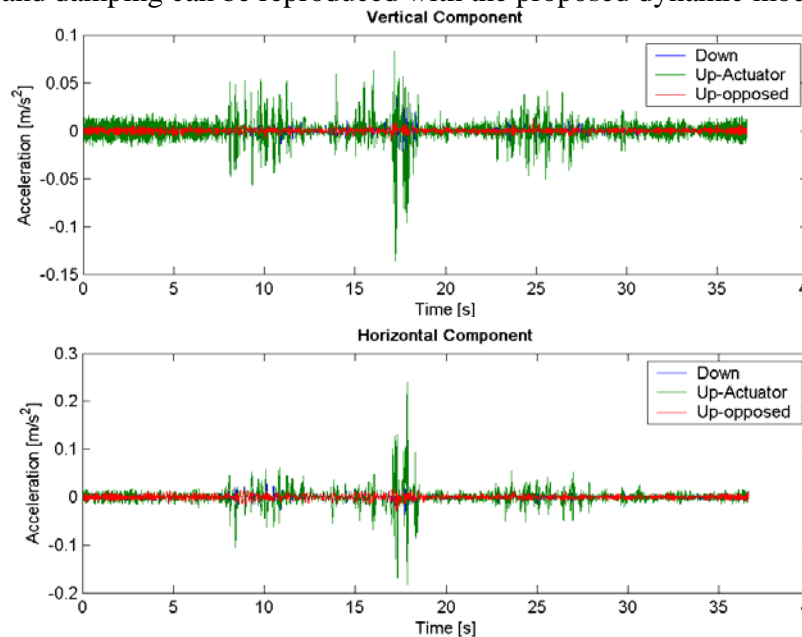


Fig. 10. Horizontal and vertical accelerations recorded by the servo-accelerometers in the three main locations on the reaction mass. With reference to Fig. 8, the label “down” refers to location C, “up-actuator” to B, and “up-opposed” to A

Some configurations of springs and dashpots were studied in order to optimize the simulation of the measured responses at both sides of the reaction mass, in the horizontal and vertical directions. However, the results presented in this section do not refer to the optimal configuration of springs and dashpots that works for any test or input signal. Additional experimental tests are required to validate the studied configuration and much more rigorous optimization methods (e.g., least-squares identification [16]) have to be introduced for defining the optimal solutions. The initial values for the total horizontal and vertical springs and dashpots are those estimated as the “average” values introduced in Section 3.3 for the comparison with the model of the design phase of the dynamic testing facility (Table 1). Initially, the stiffness coefficient associated to each spring was assumed equal the total value divided by the number of springs (ns); similarly for the nd dashpots.

As already introduced in Section 4.1, the input signal applied during the tests listed in Table 1 is not available. Therefore, the Coalinga record considered during the numerical simulations is the input already used for reproducing the results discussed in Section 3.3 and it was downloaded from

[28]. In addition, comparing the velocity and accelerations time-histories of Test N°1 versus Test N°2, it seems that the record that was applied during the two tests could not be exactly the same. For this reason and for the uncertainty related to the lack of correlation between the velocities (Fig. 9) and the accelerations (Fig. 10), the comparison between the numerical and the experimental results is performed considering the peak response quantities from the analysis and results from the tests.

The results summarised in Table 2 have been obtained with uniform distributed springs and dashpots. Considering the horizontal components, the acceleration computed in A is greater than the one obtained at location B, and this disagrees with the signal attenuation observed during the experimental test moving from location B to A (labelled as “up-actuator” and “up-opposed in Fig. 10). The same conclusion can be applied to the vertical components since the computed responses in A and in B reach the same order of magnitude. After these considerations, different weights have been assigned to the springs and dashpots in both horizontal and vertical directions in order to reproduce the observed responses as well as the rocking of the reaction mass. The first comparison with the measured signals refers to the horizontal and vertical velocities at point B, that is at the actuator anchorage zone (Fig. 8a). Table 3 compares, in term of peak values, the numerical solutions of the proposed mathematical model with the available experimental responses. The proposed model results in good correlation in term of ratio of computed to observed peak response, mainly for the horizontal component of the velocity.

Table 2. Attenuation estimate of the peak accelerations at locations B and A (labelled as “up-actuator” and “up-opposed in Fig. 10) obtained solving the proposed model with uniformly distributed springs and dashpots. Comparison with the acquired experimental responses in B

<i>Acceleration component</i>	<i>Peak value</i>	<i>Numerical response in B (m/s²)</i>	<i>Numerical response in A (m/s²)</i>	<i>Experimental response in B (m/s²)</i>	<i>Ratio Num.in A/ Num. in B</i>	<i>Ratio Num.in B/Exp.</i>
Horizontal	Positive	+0.192	+0.243	+0.229	1.27	0.84
	Negative	-0.207	-0.261	-0.189	1.26	1.10
Vertical	Positive	+0.060	+0.065	+0.087	1.08	0.69
	Negative	-0.064	-0.061	-0.131	0.96	0.49

Table 3. Comparisons of the peak velocities: solutions of the proposed model vs acquired experimental responses (plotted in Fig. 9 on the left, location B)

<i>Velocity component</i>	<i>Peak value</i>	<i>Numerical response (mm/s)</i>	<i>Experimental response (mm/s)</i>	<i>Ratio Num./Exp.</i>
Horizontal	Positive	+4.373	+3.939	1.11
	Negative	-4.517	-4.343	1.04
Vertical	Positive	+2.109	+1.495	1.40
	Negative	-2.346	-1.677	1.39

Table 4. Comparisons of the peak accelerations: solutions of the proposed model vs acquired experimental responses (plotted in Fig. 10, at location B labelled as “Up-actuator”)

<i>Acceleration component</i>	<i>Peak value</i>	<i>Numerical response (m/s²)</i>	<i>Experimental response (m/s²)</i>	<i>Ratio Num./Exp.</i>
Horizontal	Positive	+0.206	+0.229	0.90
	Negative	-0.197	-0.189	1.04
Vertical	Positive	+0.113	+0.087	1.30
	Negative	-0.122	-0.131	0.89

The second step of the validation is related to the comparisons between simulated and measured accelerations. Considering the acceleration at the actuator side (location B or “up-actuator”), comparisons of the computed and experimental peak values are given in Table 4. The proposed

model provides reasonably good correlation to the experimental test data, resulting in better accuracy if the horizontal component is considered. Despite the overestimation of the vertical components, comparison with the experimental results shows noticeable improvement in response predictions when a uniform configuration of springs and dashpots (last column of Table 2) is replaced by a non-uniform distribution of the stiffness and damping of the soil (last column of Table 4). In terms of peak values, the obtained results are able to capture the responses measured during the experimental test, in the vertical and horizontal direction, respectively. It is important to remind that the amplitudes of the computed velocities and accelerations depend on to the assigned distribution of both springs and dashpots representing the soil, which is not the optimal configuration since additional test data are required. After the performed comparisons, it could be stated that the numerical results are promising since they are capable to capture the complex behaviour of a large dynamic testing facility whose response is difficult to understand and be accurately reproduced from the available experiments.

5. CONCLUSIONS

The present research featured the objective of developing a mathematical model for a large dynamic testing facility. Using the Lagrange's formulation, a system of four nonlinear second-order differential equations was derived and formulated in a general manner in order to catch the behaviour of a generic large-scale dynamic testing facility with motion allowed in the longitudinal direction and to consider the effects of the nonlinear kinematics due to possible large rotations.

The accuracy of the equations of motion was firstly checked with preliminary numerical verifications and then against the experimental results of the large uniaxial shake table built in the EUCENTRE Laboratory. During this validation phase, several limitations of the available experimental data were encountered. Therefore, the validation was not straightforward and the collected tests do not represent an exhaustive set of examples for validating the model. A preliminary calibration procedure was carried out in order to take into account the non-uniform distribution of stiffness and damping of the surrounding soil and to capture the rocking that characterises the motion of the reaction mass. Nonetheless, additional experimental data are required for calibrating the analytical model and characterising the motion of the dynamic facility.

The preliminary numerical validations seem very promising. Therefore, after the implementation of more sophisticated optimisation methods required to reduce the fit error, the developed analytical model may perhaps accurately reproduce the real behaviour of a large dynamic testing facility. Finally, future work is also to be carried out for the analysis of solution sensitivity to initial conditions in order to evaluate the importance of the initial conditions to the final solutions.

ACKNOWLEDGEMENTS

The authors thank Mr. J. Londono Bustamante, Mr. F. Dacarro, Mr. R. Franzolin, Dr. A. Pavese and Dr. C. Strobbia for the assistance in retrieving experimental data related to the case-study considered in this research work.

REFERENCES

1. Merritt HE. *Hydraulic Control Systems*, John Wiley & Sons, New York, 1967.
2. Rea D, Abedi-Hayati S, Takahashi Y. Dynamic analysis of electro-hydraulic shaking tables. *EERC Report No. 77/29*, Earthquake Engineering Research Center, University of California at Berkeley, California, USA, 1977.
3. Blondet M, Esparza C. Analysis of shaking table-structure interaction effects during seismic simulation tests, *Earthquake Engineering and Structural Dynamics* 1988; **16**: 473-490.
4. Rinawi AM, Clough RW. Shaking table-structure interaction. *EERC Report No. 91/13*, Earthquake Engineering Research Center, University of California at Berkeley, California, USA, 1991.

5. Muhlenkamp M, Conte JP, Hudgings TR, Durrani AJ. Analysis design, and construction of a shaking table facility. Structural Research at Rice, *Report No. 46*, Department of Civil Engineering, Rice University, Houston, Texas, USA, 1997.
6. Dai H, Sain MK, Spencer BF Jr. Using sensors to track earthquakes on hydraulic shaker tables. *Proceedings of the American Control Conference*, IEEE, Piscataway NJ, 1997; Part 1: 1-5.
7. Conte JP, Trombetti TL. Linear dynamic modeling of a uniaxial servo-hydraulic shaking table system. *Earthquake Engineering and Structural Dynamics* 2000; **29**(9): 1375-1404.
8. Ozelik O, Luco JE, Conte JP, Trombetti TL, Restrepo JI. Experimental characterization, modelling and identification of the NEES-UCSD shake table mechanical system. *Earthquake Engineering and Structural Dynamics* 2008; **37**: 243-264.
9. Plummer AR. Control techniques for structural testing: a review, *Proceedings of the Institution of Mechanical Engineers, Part I.: Journal of Systems and Control Engineering* 2007; **221**(2): 139-169.
10. Severn RT. Earthquake Engineering Research Infrastructures, *Structural Engineering, Mechanics and Computation*, Editor Zingoni A, Elsevier Science, 2001; **1**: 195-209.
11. Füllekrug U. Utilisation of multi-axis shaking tables for the modal identification of structures, *Philosophical Transactions of the Royal Society A: Mathematical, Physical & Engineering Sciences* 2001; **359**(1786): 1753-1770.
12. Severn RT. The development of shaking tables – A historical note, *Earthquake Engineering and Structural Dynamics*, 2010; DOI: 10.1002/eqe.1015.
13. Williams MS, Blakeborough A. Laboratory testing of structures under dynamic loads: an introductory review, *Philosophical Transactions of the Royal Society A: Mathematical, Physical & Engineering Sciences* 2001; **359**(1786): 1651-1669.
14. Stoten DP, Gómez EG. Adaptive control of shaking tables using the minimal control synthesis algorithm, *Philosophical Transactions of the Royal Society A: Mathematical, Physical & Engineering Sciences* 2001; **359**(1786): 1697-1723.
15. Calvi GM, Pavese A, Ceresa P, Dacarro F, Lai CG, Beltrami C. *Design of a Large-Scale Dynamic and Pseudo-Dynamic Testing Facility*, IUSS Press, Pavia, Italy, 2005.
16. Franklin GF, Powell JD, Emami-Naeini A. *Feedback Control of Dynamic Systems*, third ed., Addison-Wesley Publishing Company, United States of America, 1994.
17. D’Azzo JJ, Houpis CH. *Feedback Control System Analysis & Synthesis*, second ed., International Student Edition, McGraw-Hill Electrical and Electronic Engineering Series, Tokyo, Japan, 1966.
18. Clark AJ. Dynamic characteristics of large multiple degree of freedom shaking tables, *Proceedings of the 10th World Conference on Earthquake Engineering*, Madrid, Spain, 1992; 2823-2828.
19. Crewe AJ, Severn RT. The European collaborative programme on evaluating the performance of shaking tables, *Philosophical Transactions of the Royal Society A: Mathematical, Physical & Engineering Sciences* 2001; **359**(1786): 1671-1696.
20. Goldstein H. *Meccanica classica*, Zanichelli Bologna (in Italian), 1994.
21. Legnani G, Righettini P, Zappa B, Casolo F. A Homogeneous Matrix Approach to 3D Kinematics and Dynamics. Part 1: Theory, *Mechanism and Machine Theory* 1996; **31**(5): 573-587.
22. Legnani G. *Robotica Industriale*, Casa Ed. Ambrosiana (in Italian), Italy, 2003.
23. The MathWorks, Inc. Matlab, The Language of Technical Computing, Version 6.5.0.180913a, Release 13, 2002.
24. Chopra AK. *Dynamics of structures*, second ed., Prentice Hall, Upper Saddle River, United States of America, 2001.
25. Pavese A, Peloso S, Bolognini D. FRP seismic retrofit of RC square hollow section bridge piers, *Journal of Earthquake Engineering* 2004; **8**(1), 225-250.
26. DIET, Misura delle variazioni di quota dei punti di controllo situati sul basamento della tavola vibrante, *Research report* (in Italian), Dipartimento di Ingegneria Edile e del Territorio, Università degli Studi di Pavia, 2007.
27. Londono J. Dynamic response of soil under vibrations produced by the EUCENTRE shaking table, *MsC Thesis* (in preparation), ROSE School, Pavia, Italy.
28. PEER Strong Motion Database (online). Available from the URL: <http://peer.berkeley.edu/smcat/>, 2000.